Structures and transport properties of polycrystalline Fe_3O_4 films

2003 J. Phys.: Condens. Matter 15 8003

(http://iopscience.iop.org/0953-8984/15/46/016)

INSTITUTE OF PHYSICS PUBLISHING JOURNAL OF PHYSICS: CONDENSED MATTER

J. Phys.: Condens. Matter **15** (2003) 8003–8009 PII: S0953-8984(03)65879-0

Structures and transport properties of polycrystalline Fe_3O_4 films

Hui Liu[1], E Y Jiang[1], R K Zheng[2] and H L Bai[1,3]

[1] Institute of Advanced Materials Physics and Faculty of Science and Key Laboratory for Advanced Ceramics and Machining Technology, Tianjin University, Tianjin 300072, People's Republic of China
[2] Department of Physics and Institute of Nanoscience and Technology, The Hong Kong University of Science and Technology, Hong Kong, People's Republic of China

E-mail: baihaili@public.tpt.tj.cn

Received 6 July 2003, in final form 1 October 2003
Published 7 November 2003
Online at stacks.iop.org/JPhysCM/15/8003

Abstract

Polycrystalline Fe_3O_4 films have been prepared by reactive sputtering at room temperature. A transmission electron microscope image shows that the films consist of Fe_3O_4 grains well separated by grain boundaries with long-range and atomic scale disorders. The width of the long-range disordered grain boundaries observed by high resolution transmission electron microscopy is about ∼4 nm, which is consistent with the boundary dimension derived from the resistivity and magnetization measurements. The temperature dependence of resistivity indicates that the transport properties of the films are dominated by the mechanism of fluctuation-induced tunnelling of electrons across the grain boundaries. Ordinary and extraordinary Hall constants were measured to be -8.22×10^{-11} and $\sim -1.45 \times 10^{-8}$ Ω cm G^{-1}, which are two and three orders of magnitude larger than those of iron, respectively.

1. Introduction

Inverse spinel structured magnetite (Fe_3O_4) has attracted much attention due to its half metallicity with 100% spin polarization which, principally, may cause significant tunnel magnetoresistance (TMR) [1–3]. This property, together with its high Curie temperature ($T_C = 850$ K), relatively low deposition temperatures, and its ability to make ultra-thin Fe_3O_4 films with nearly unchanged magnetic properties, have made Fe_3O_4 a promising candidate for TMR devices [4]. Accordingly, TMR of different forms of Fe_3O_4 has been extensively studied recently, including single crystal [4–10] and polycrystalline [7, 12] films, powders [7, 12, 13] and junctions involving Fe_3O_4 as electrodes [14–16]. It has been realized that as tunnelling barriers, grain boundaries are of fundamental importance to the TMR effect

[3] Author to whom any correspondence should be addressed.

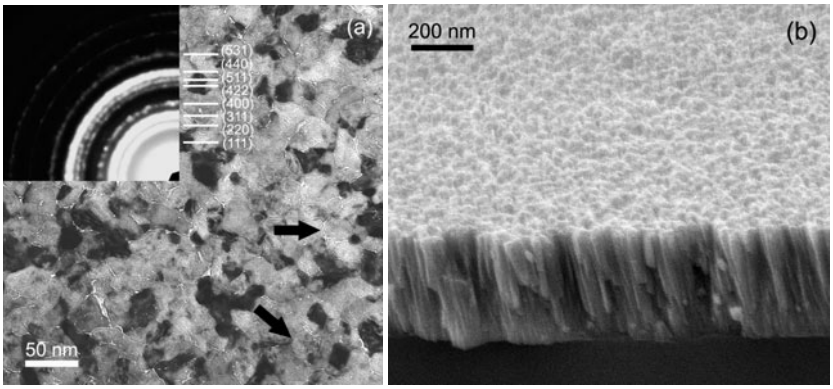

Figure 1. (a) TEM bright field image and SAED pattern and (b) cross-sectional SEM image of 330 nm thick Fe_3O_4 film. The arrows in (a) indicate two types of grain boundaries shown in figure 3.

of Fe_3O_4 polycrystalline films and powders. However, the role of grain boundaries in the magnetotransport properties remains poorly understood due to the difficulty of discriminating between many factors that influence the magnetoresistance (MR), such as magnetic impurities, structural disorder and interface roughness, etc [13]. With a better understanding of the nature of the boundaries, it may be possible to further exploit the grain-boundary properties for practical applications. In this paper, we report the structures, especially the microstructures of the grain boundaries of the polycrystalline Fe_3O_4 films deposited by reactive sputtering at room temperature (RT), and their transport properties such as resistivity and Hall effect that can give information on carrier type and density.

2. Experiment

The Fe_3O_4 films were fabricated by magnetron sputtering a Fe target in a $Ar + O_2$ mixture on glass and kapton substrates at RT. The background pressure of the chamber is better than 1.33×10^{-5} Pa. The film thickness was measured by a Dektak 3 surface profiler. The structures of the films were characterized by x-ray diffraction (XRD), transmission electron microscopy (TEM) and scanning electron microscopy (SEM). The chemical states were analysed by x-ray photoelectron spectroscopy (XPS). The resistance and Hall resistance of the films were measured with the standard four- and five-probe methods respectively, in a magnetic field of -50 kOe $\leqslant H \leqslant 50$ kOe and at temperatures ranging from 1.8 to 300 K using a Quantum Design MPMS-5S superconducting quantum interference device (SQUID) magnetometer.

3. Results and discussion

Figure 1(a) shows the bright field image and selected area diffraction (SAED) pattern of 330 nm Fe_3O_4 film. One can see that the film is polycrystalline and Fe_3O_4 grains are well separated by grain boundaries. By the linear intercept method, i.e. from the number of line crossings, the average lateral grain size was measured to be $\sim$25 nm. Figure 1(b) shows the cross-sectional SEM image of the 330 nm Fe_3O_4 film, indicating a column structure. It is worth mentioning here that because γ-Fe_2O_3 (maghemite) has the same cubic inverse spinel structure and nearly

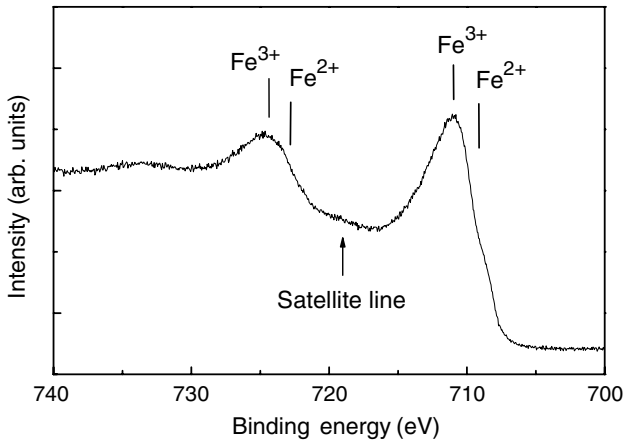

Figure 2. XPS spectrum of 330 nm thick Fe_3O_4 film taken at $h\nu = 1253.6$ eV.

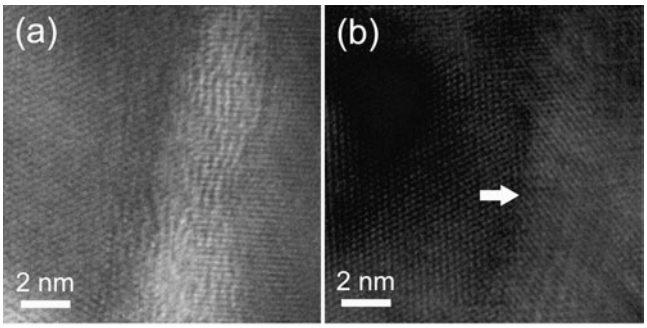

Figure 3. HRTEM images of the grain boundaries with (a) long-range and (b) atomic scale disorders. The long-range and atomic scale disorders are labelled by the top and bottom arrows in figure 1(a), respectively.

the same lattice parameter ($a = 0.8350$ nm) as Fe_3O_4 ($a = 0.8396$ nm), the diffraction rings can not only be indexed to polycrystalline Fe_3O_4 but also to polycrystalline γ-Fe_2O_3, or their mixture. In order to further clarify the phases presented in the films, XPS was performed to analyse the chemical states of iron. Figure 2 shows the Fe 2p core-level photoemission spectrum of the Fe_3O_4 film taken at $h\nu = 1253.6$ eV. Due to spin–orbit coupling, the Fe 2p core levels split into $2p^{1/2}$ and $2p^{3/2}$ components, situated at about 711 and 724 eV, respectively. The broadening of the Fe $2p^{1/2}$ and Fe $2p^{3/2}$ peaks indicates the existence of Fe^{2+}. The absence of satellite line situated at about 719 eV, which is characteristic of Fe^{3+} in γ-Fe_2O_3, suggests that γ-Fe_2O_3 does not exist in the films.

Further investigation of the microstructures of the grain boundaries was performed by high resolution transmission electron microscopy (HRTEM). Figure 3 shows the HRTEM images of two types of boundaries, which are indicated in figure 1(a) by two arrows. From figure 3(a), one can see that the microstructure of the ∼4 nm long-range disordered region between two Fe_3O_4 grains (labelled by the top arrow in figure 1(a)) is different from that in grains. On the other hand, as shown in figure 3(b), the lattice image of the other type of boundary (labelled by the bottom arrow in figure 1(a)) is local disordered on atomic scale. Most grains in the Fe_3O_4

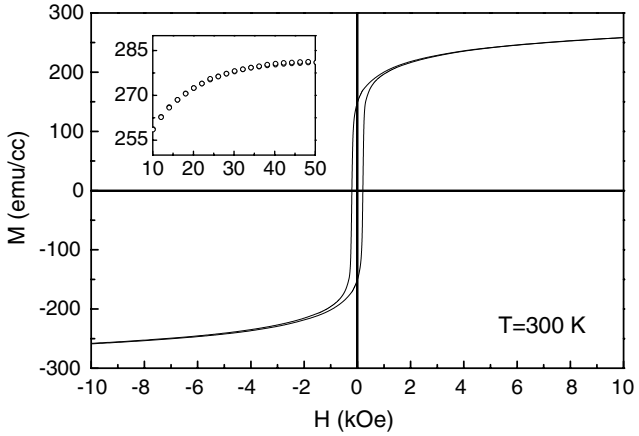

Figure 4. Magnetization loop for 330 nm thick Fe_3O_4 film measured at 300 K. The inset shows part of the first quadrant loop.

film are connected by the long-range disordered boundaries, as shown in figure 1(a). These two types of boundary can make the intrinsic and extrinsic properties of our Fe_3O_4 films, such as stress/strain, reconstructions, non-stoichiometry and interdiffusion, etc, be quite different from those of bulk material, and cause spin disorder in the regions, which can significantly alter the transport and the magnetic properties of the polycrystalline films.

Figure 4 shows the magnetization loop of the 330 nm Fe_3O_4 sample measured at 300 K. At 50 kOe, the magnetization is about 280 emu cm^{-3} and not saturated even at such a high field. This value is much less than the saturation magnetization of 471 emu cm^{-3} measured at 300 K for some single crystalline films and bulk Fe_3O_4 [17, 18]. Similar magnetization behaviour has also been observed in other nanocrystalline Fe_3O_4 films, where the magnetization is about ∼70% of the bulk value [11, 13]. We suggest that the magnetization reduction is caused by the strong anti-ferromagnetic (AF) coupling within grain boundaries due to the surface imperfection induced spin disorder such as oxygen deficiency, impurity, etc [19]. With the decrease of film thickness, the magnetization measured at 50 kOe decreases due to (1) the increased density of the AF grain boundary caused by grain size reduction and (2) the increased contribution of surface layer with lower magnetization. By simply assuming that the spherical Fe_3O_4 core is coated by the shell of the boundary, and taking a magnetization ratio of $M_{\text{film}}/M_{\text{bulk}} \sim 60\%$ as the volume ratio of the Fe_3O_4 cores, we calculate the dimension ratio of the core to the shell to be ∼6.25, which is consistent with the linear ratio of grain size (∼25 nm) to boundary width (∼4 nm) obtained above. This means that the long-range disordered boundaries are dominant in the Fe_3O_4 films, as evidenced in figure 1.

Shown in figure 5 is the $\log \rho$ versus T curve for the Fe_3O_4 film. Those of thinner films show similar tendencies except for higher resistivity due to enhanced interface (grain boundary) and surface scattering (not shown). It is noteworthy that (1) at 300 K, the lowest resistivity is $\sim 1.8 \times 10^5$ $\mu\Omega$ cm, which is about one order larger than that of some epitaxial Fe_3O_4 single crystal films [1, 6, 7], and (2) the Verwey transition that is usually observed in the $\log \rho$ versus T relation of the Fe_3O_4 system does not appear. This high resistivity, as well as the absence of the Verwey transition, suggests that the resistivity of our Fe_3O_4 films is grain boundary controlled. In order to further understand the mechanism that dominates the transport process, as shown in the inset of figure 5, the temperature dependence of resistivity is replotted as $\log \rho \sim T_1/(T + T_2)$. It is seen that the experimental data can be well fit by

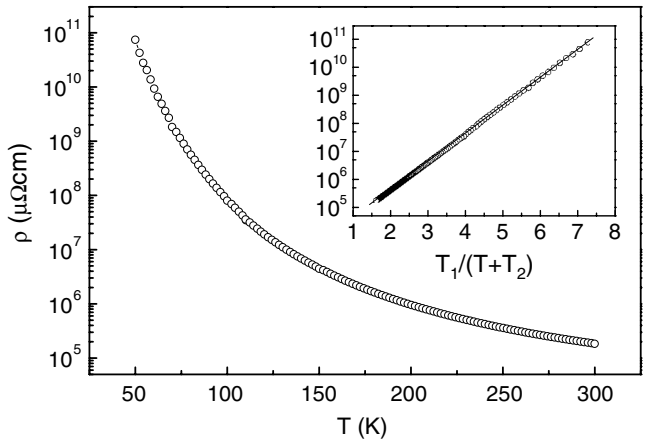

Figure 5. Temperature dependence of resistivity. The inset shows a $\log \rho \sim T_1/(T + T_2)$ plot with $T_1 = 521$ K and $T_2 = 22$ K.

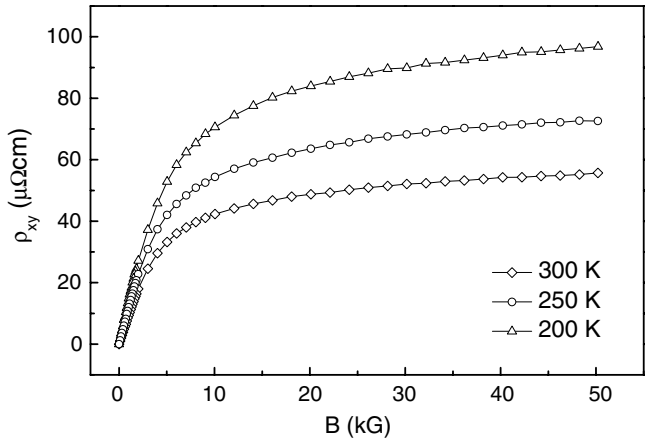

Figure 6. Hall resistivities measured at different temperatures.

$\rho \propto \rho_0 \exp[T_1/(T + T_2)]$ with $T_1 = 521$ K and $T_2 = 22$ K, which is in agreement with the prediction of the fluctuation-induced tunnelling model [20, 21]. This semi-classical model is based on thermal fluctuations of electric potential $\delta u \sim (kT/C)^{1/2}$ on the edges of a tunnelling gap with the capacitance C. The product χw, where χ is the tunnelling constant and w the typical tunnelling distance (or the width of junction gap), can be estimated from the relation $T_1/T_2 = \pi \chi w/2$. By using the fitting parameters T_1 and T_2 and assuming that the localization length $1/\chi$ is about 0.2–0.3 nm (or of the order of the extension of electron wavefunctions out of metal into vacuum) [20–22], the corresponding tunnelling distance (or the average thickness of grain boundaries) was calculated to be 3–4 nm, which is in good agreement with the boundary width obtained by HRTEM, confirming that the density of the long-range disordered boundaries is much larger than that of atomic scale disordered boundaries. This result also means that the conduction electrons tunnel through ~5 unit cells of Fe_3O_4 ($a = 0.8396$ nm) during the transport between adjacent grains.

Ordinary and extraordinary Hall coefficients were also measured in order to gain a deeper understanding of the transport properties of the polycrystalline Fe_3O_4 films. Figure 6 shows

the Hall resistivity (absolute value) versus magnetic field at 200, 250 and 300 K for the 330 nm thick Fe_3O_4 film. The saturated anomalous Hall resistivity at 200 and 300 K is about -81.1 and -45.9 $\mu\Omega$ cm, respectively. The minus sign of both ordinary and extraordinary Hall resistivity suggests an electron dominant transport mechanism. As the magnetization does not saturate even at high magnetic fields within our measurement field of 50 kOe, we cannot simply obtain the ordinary and extraordinary Hall coefficients by extrapolating the linear parts of the curves from high field to zero. For magnetic materials, the Hall resistivity can be described by the phenomenological relation of $\rho_{xy} = R_0 B + R_s 4\pi M$ [23], where $B = H + 4\pi M$, R_0 is the ordinary Hall coefficient and R_s the extraordinary Hall coefficient. By substituting the values of B and $4\pi M$ at $H = 40$ and 50 kOe into the relation and solving two equations, we obtained the ordinary and extraordinary Hall coefficients of $R_0 = 8.22 \times 10^{-11}$ Ω cm G^{-1} and $R_s = 1.45 \times 10^{-8}$ Ω cm G^{-1}, respectively, which gives the carrier density of $n = 1/(R_0 e) \sim 7.6 \times 10^{26}$ m^{-3}. The ordinary and extraordinary Hall coefficients at 300 K are about 357 and 2014 times larger than those of iron ($R_0 = 0.23 \times 10^{-12}$ Ω cm G^{-1}, $R_s = 7.2 \times 10^{-12}$ Ω cm G^{-1}) and also higher than those of polycrystalline Fe_3O_4 films reported previously [23, 24].

In fact, the giant enhancement of the Hall effect has never been observed in other inhomogeneous systems such as NiFe–SiO_2, Ni–SiO_2, Co–SiO_2 and Cu–SiO_2 [25–28]. The anomalous Hall resistivity observed in NiFe–SiO_2 films is up to 160 $\mu\Omega$ cm at 5 K near the percolation threshold, which is almost four orders of magnitude larger than that in corresponding pure metal [25]. A nearly three orders of magnitude enhancement of the Hall constant was observed at 5 K near the percolation threshold in the Cu–SiO_2 system as the Cu volume fraction decreased [28]. It has been suggested theoretically that the origin of the giant Hall effect (GHE) for polarized electrons is from the co-contribution of quantum interference and spin–orbit interactions [29], and has been adopted to explain the GHE observed in inhomogeneous magnetic systems [30, 31]. Bearing in mind that our Fe_3O_4 system is microscopically inhomogeneous, and the electron transport is dominated by spin-dependent tunnelling [19], we suggest that the observed enhancement of the Hall constants in our Fe_3O_4 system may come from these two mechanisms.

4. Conclusion

Polycrystalline Fe_3O_4 films with Fe_3O_4 grains separated by the long-range and atomic-scale disordered grain boundaries have been prepared by reactive sputtering at RT. Both resistivity and magnetization measurements give a ~4 nm grain-boundary region, indicating that the long-range disordered boundaries are dominant in the films, as evidenced by TEM observations. The electron transport process is dominated by the fluctuation-induced tunnelling mechanism. At RT, the saturated Hall resistivity is ~ -45.9 $\mu\Omega$ cm, and ordinary and extraordinary Hall constants are $\sim -8.22 \times 10^{-11}$ and $\sim -1.45 \times 10^{-8}$ Ω cm G^{-1}, respectively. The enhancement in the ordinary and extraordinary Hall constants compared to those of iron is suggested to be attributed to the co-contribution of quantum interference and spin–orbit interactions.

Acknowledgments

The authors are grateful to Dr X X Zhang, Hong Kong University of Science and Technology, for his cooperation in carrying out the SQUID measurements. The work was financially supported by the following grants: National Science Foundation of China (50172033), Excellent Researcher Training Project for 21st Century, Key Project of Science and Technology,

Key Teacher Supporting Project, SRF for ROCS of State Education Ministry, and Science Foundation of Tianjin Education Committee (no 01-20415).

References

[1] Verwey E J W 1939 *Nature* **144** 327
[2] Yanase Y and Siratori K 1984 *J. Phys. Soc. Japan* **53** 312
[3] Zhang Z and Satpathy S 1991 *Phys. Rev.* B **44** 13319
[4] Soeya S, Hayakawa J, Takahashi H, Ito K, Yamamoto C, Kida A, Asano H and Matsui M 2002 *Appl. Phys. Lett.* **80** 823
[5] Margulies D T, Parke F T, Rudee M L, Spada F E, Chapman J N, Aitchison P R and Berkowitz A E 1997 *Phys. Rev. Lett.* **79** 5162
[6] Gong G Q, Gupta A, Xiao G, Qian Q and Dravid V P 1997 *Phys. Rev.* B **56** 5096
[7] Coey J M D, Berkowitz A E, Balcells L, Putris F F and Parker F T 1998 *Appl. Phys. Lett.* **72** 734
[8] Voogt F C, Palstra T T M, Niesen L, Rogojanu O C, James M A and Hibma T 1998 *Phys. Rev.* B **57** R8107
[9] Ziese M and Blythe H J 2000 *J. Phys.: Condens. Matter* **12** 13
[10] Eerenstein W, Palstra T T M, Saxena S S and Hibma T 2002 *Phys. Rev. Lett.* **88** 247204
[11] Furubayashi T 2003 *J. Appl. Phys.* **93** 8026
[12] Peng D L, Asai T, Nozawa N, Hihara T and Sumiyama K 2002 *Appl. Phys. Lett.* **81** 4598
[13] Venkatesan M, Nawka S, Pillai S C and Coey J M D 2003 *J. Appl. Phys.* **93** 8023
[14] Li X W, Gupta A, Xiao Q, Qian W and Dravid V P 1998 *Appl. Phys. Lett.* **73** 3282
[15] Seneor P, Fert A, Maurice J-L, Montaigne F, Petroff F and Vaurès A 1999 *Appl. Phys. Lett.* **74** 4017
[16] Hu G and Suzuki Y 2002 *Phys. Rev. Lett.* **89** 276601
[17] Bickford L R Jr 1950 *Phys. Rev.* **78** 449
[18] Sangeeta K, Bhagat S M, Lofland S E, Scabarozi T, Ogale S B, Orozco A, Shinde S R, Venkatesan T, Hannoyer B, Mercey B and Prellier W 2001 *Phys. Rev.* B **64** 205413
[19] Liu H, Jiang E Y, Bai H L, Zheng R K, Wei H L and Zhang X X 2003 *Appl. Phys. Lett.* **83** 3531
[20] Sheng P, Sishel E K and Gittleman J I 1978 *Phys. Rev. Lett.* **40** 1197
[21] Sheng P 1980 *Phys. Rev.* B **21** 2180
[22] Pakhomov A B, Zhang X X, Liu H, Wang X R, Huang H J and Yang S H 2000 *Physica* B **279** 41
[23] Berger L and Bergmann G 1979 *The Hall Effect and Its Applications* ed C L Chien and C R Westgate (New York: Plenum) p 55
Berger L and Bergmann G 1999 *Modern Magnetic Materials Principles and Applications* ed R C O'Handley (New York: Wiley–Interscience) p 570
[24] Feng J S-Y, Pashley R D and Nicolet M-A 1975 *J. Phys. C: Solid State Phys.* **8** 1010 and references therein; note that the definition of the extraordinary Hall coefficient is different from that in this paper by 4π
[25] Pakhomov A B and Yan X 1996 *Solid State Commun.* **99** 139
[26] Pakhomov A B, Yan X and Zhao B 1995 *Appl. Phys. Lett.* **67** 3497
[27] Denardin J C, Pakhomov A B, Knobel M, Liu H and Zhang X X 2000 *J. Phys.: Condens. Matter* **12** 3397
[28] Zhang X X, Wan C C, Liu H, Li Z Q, Sheng P and Lin J J 2001 *Phys. Rev. Lett.* **86** 5562
[29] Holstein T 1961 *Phys. Rev.* **124** 1329
[30] Aronzon B A, Kovalev D Y, Lagarkov A N, Meilikhov E Z, Rylkov V V, Sedova M A, Negre N, Goiran M and Leotin J 1999 *JETP Lett.* **70** 90
[31] Aronzon B A, Meilikhov E Z, Rylkov V V, Lagarkov A N, Sedova M A, Evstushina I A, Kovalev D Y, Vegre N, Goiran M and Leotin J 2000 *Physica* B **284** 1980